UNIVERSITY OF OULU

FACULTY OF INFORMATION TECHNOLOGY AND ELECTRICAL ENGINEERING

DEGREE PROGRAMME IN ELECTRONICS AND COMMUNICATIONS ENGINEERING

MASTER'S THESIS

INKJET-PRINTED SWCNT CONDUCTORS AND SENSORS ON PDMS

Author	Henri Ervasti
Supervisor	Krisztián Kordás
Second Examiner	Olli Pitkänen
Technical Advisor	Topias Järvinen

June 2020

Ervasti H. (2020) Inkjet-Printed SWCNT Conductors and Sensors on PDMS. University of Oulu, Faculty of Information Technology and Electrical Engineering, Degree Programme in Electronics and Communications Engineering. Master's Thesis, 38 p.

ABSTRACT

Inkjet printing of single-wall carbon nanotubes (SWCNT) on flexible polydimethylsiloxane (PDMS) substrates and their electrical properties were studied in this thesis. Wetting of the surface of the substrate with custom-made dimethylformamide-based conductive SWCNT ink was optimized by using argon-plasma surface treatment. Conductive micropatterns of SWCNTs were obtained. Mechanical bending and stretching experiments showed deformation dependent transport behaviour with a large pressure sensitivity and a gauge factor of up to 1000. The printed micropatterns were found to be sufficiently sensitive to detect and resolve pressure fronts of heartbeats in a human radial artery. Due to the established manufacturing processes used: inkjet- and screen printing, the study can pave the way for the integration of piezoresistive sensors in flexible and stretchable devices to be used e.g. in medical garments, sportswear and their accessories.

Keywords: Flexible, stretchable, polymer, inkjet printing, piezoresistive, transparent.

Ervasti H. (2020) Mustesuihkutulostetut yksiseinämäiset hiilinanoputkijohteet ja -anturit polydimetyylisiloksaanilla. Oulun yliopisto, Tieto- ja sähkötekniikan tiedekunta, Elektroniikan ja tietoliikennetekniikan tutkinto-ohjelma. Diplomityö, 38 s.

TIIVISTELMÄ

Tässä työssä tutkittiin yksiseinämäisten hiilinanoputkien (SWCNT) mustesuihkutulostamista joustavalle polydimetyylisiloksaanista (PDMS) valmistetulle substraatille sekä niiden sähköisiä ominaisuuksia. Erikoisvalmisteisen dimetyyliformamidipohjaisen johtavan SWCNT-musteen substraatin pinnan kostutusta optimoitiin argon plasma pintakäsittelyllä. Tuloksena saatiin monipuolisia johtavia SWCNT-mikrokuvioita. Taivutettaessa ja venytettäessä kuviot osoittivat muodonmuutoksesta riippuvaa johtavuuden vaihtelua suurella paineherkkyydellä ja jopa yli tuhannen venymäkertoimella (Gauge Factor). Mikrokuviot olivat riittävän herkkiä myös havaitsemaan ja tulkitsemaan sydämen sykkeen aiheuttaman paineenvaihtelun ihmisen rannevaltimosta. Vakiintuneiden valmistusmenetelmien, mustesuihkutulostuksen ja silkkipainon käytön takia, tutkimus voi tasoittaa tietä kohti taipuvissa ja venyvissä laitteissa käytettävien pietsoresistiivisten antureiden integrointia esimerkiksi lääketieteellisiin ja urheilutekstiileihin ja –tarvikkeisiin.

Avainsanat: Joustava, venynvä, polymeeri, mustesuihkutulostus, pietsoresistiivinen, läpinäkyvä.

TABLE OF CONTENTS

ABBREVIATIONS

TCF	transparent conductive film
LCD	liquid crystal display
PET	polyethylene terephthalate
CNT	carbon nanotube
SWCNT	single-wall carbon nanotube
MWCNT	multi-walled carbon nanotube
DMF	dimethylformamide
SWCNT-COOH	carboxylic acid functionalized single-wall carbon nanotube
sccm	standard cubic centimeters per minute
mTorr	milliTorr (unit of pressure)
rpm	revolutions per minute
Ω/sq	ohms per square, unit of sheet resistance
FESEM	field-emission scanning electron microscopy
AFM	atomic force microscopy
I-V	current-voltage
DC	direct current
GF	gauge factor
UV-Vis-NIR	ultraviolet-visible-near-infrared
FFT	fast Fourier transform
DMM	digital multimeter
R2R	roll-to-roll
DI water	deionized water

FOREWORD

This thesis is based on the work carried out in the Microelectronics Research Unit and supported by projects: Flexibla Transparenta Ledande Filmer som Electroder (EU Interreg Nord and Lapin liitto) and Nigella (Academy of Finland)

I thank my Supervisor professor Krisztián Kordás for his guidance, my Technical Advisor Topias Järvinen, who helped me with inkjet printing, getting used to a lot of the laboratory equipment alongside a lot of great advice, my Second Examiner Dr. Olli Pitkänen for helping with cleanroom equipment, Tuomo Siponkoski for the help with Linkam stretch stage and Éva Bozó for assisting with argon plasma treatment and introducing to laboratory and imaging equipment. I would also like to thank Olli-Heikki Huttunen and professor Jussi Hiltunen for the discussion and for the substrate materials they developed at the VTT Technical Research Centre of Finland.

Furthermore, Petra Palvölgyi, Dr. Jani Peräntie, Dr. Mikko Nelo, Dr. Gabriela Lorite-Yrjänä and other staff in the laboratory are acknowledged for sharing their knowledge and experience with me not only in work-related matters but also in leisure time.

Oulu, June 2020

Henri Ervasti

1 INTRODUCTION

This work has been inspired by Ronja Valasma's Bachelor's thesis discussing on "Micropatterned transparent conductive films of single-wall carbon nanotubes on polyethylene terephthalate surfaces" which fostered new ideas on the utilization of carbon nanotube-based technologies and devices. In the current thesis, our goals are similar as in the previous study, however, we apply a few twists to explore CNT-based conductors deposited on flexible substrates: (i) inkjet printing is used to spread the SWCNTs on the substrate instead of dip coating, (ii) for substrate materials we apply revolutionary R2R printed flexible PDMS films [1] instead of PET, and (iii) we use highly concentrated dispersions of SWCNTs in DMF instead of water.

The industry around conductive patterns on transparent surfaces is under constant transformation. Today's standard for transparent conductive films, indium tin oxide (ITO), used for example to make transparent conducting films (TCFs) for liquid-crystal displays (LCDs), photovoltaic sensors or solar panels is becoming rarer and more expensive. At the same time, demand for flexible and stretchable conductors and sensors for electrical devices (e.g. in phones, apparel, sport equipment) is increasing. Therefore, more research funding is directed towards discovering alternatives to ITO. One of the most promising materials are low-dimensional carbon allotropes such as graphene and carbon nanotubes. This work concentrates on single-wall carbon nanotubes (SWCNTs) as they have excellent properties (e.g. mechanical flexibility, large aspect ratio, and good electrical conductivity) that can be exploited not only in TCFs but also in flexible and stretchable environments – both conductor and sensor applications. Although SWCNTs are more expensive than multi-walled carbon nanotubes (MWCNTs), their films and composites enable superior electrical conductivity. In addition, their smaller size and good dispersibility in some solvents make them easier to print through small nozzles of inkjet-printers.

This work shows, to our knowledge, the first fully printed flexible device that applies novel R2R printed PDMS substrates with screen-printed Ag electrodes (developed by Hiltunen's team at VTT Technical Research Centre of Finland) and inkjet-printed micro-patterns of SWCNTs working as a piezoresistive strain sensor. The presented method is scalable and of low cost, thus after further optimization can be useful for manufacturing flexible electronics devices.

2 SWCNT PROPERTIES AND INKJET PRINTING

The trade-off between optical transparency and electrical conductivity is unavoidable when engineering TCFs. Some applications, such as those in capacitive LCDs or in antistatic coatings do not require high conductivity of the films but as much optical transparency as possible. On the other hand, films that are carrying higher currents (e.g. collector electrodes in solar cells or resistive heaters in de-fogging coatings) benefit from both high conductivity and transparency. Furthermore, current trends in foldable, bendable and flexible electronics put forward also further demands on mechanical properties. For example, commonly used doped metal oxides in TCFs are brittle and do not handle bending near as well. [2]

CNTs can be used in conjunction with other materials to change their properties (e.g. in composites) or by using them on their own (e.g. films on substrates) to create, for example, connectors or sensors like in this work. Versatile possible uses and impressive properties make CNTs appealing for future applications including conductive and high-strength composites, electrodes in energy storage [3] and conversion devices [4], physical [5] and chemical sensors [6], brushed motor contacts [7], displays and radiation sources [8], semiconductor devices [9], interconnects or connectors [2]. They have also been successfully used as integrated chip cooler fins [10],acoustic transducers in both speaker and microphone applications [11] and even as cell growth scaffolds [12]. Some applications have already made it all the way into commercial products.

Nowadays, synthesis of CNTs is mainly based on three major processes: (i) catalytic chemical vapour deposition (CVD-method), (ii) laser ablation and (iii) arc discharge growth. The CVD-method is the most practical for a scale-up with its fast processing speed, affordable consumables and ability to provide comparatively pure CNTs with only some catalyst impurities. As pure SWCNTs nowadays are intended mainly for research purposes, they are very expensive, however as the SWCNTs can be synthesized indefinitely from just simple carbon precursors (hydrocarbons, alcohols), getting their price down is just a matter of demands of industries that would use those in large quantities. [13]

2.1 Carbon nanotubes

2.1.1 CNT physical and chemical properties

SWCNTs have impressive physical properties surpassing many industry-leading materials. Effective and pure manufacturing of the nanotubes and retaining the properties when used in large-scale sheets, fibers and composites are still a difficulty. Also, in some cases possible health hazards shall be considered especially if there is a chance that they can be inhaled [14].

Some of the appealing features include: Young's modulus of 0.64 TPa for individual nanotubes, accompanied with ~50-fold density-normalized strength and ~20-fold density-normalized modulus compared to steel. A significant challenge is to achieve similar values in a macroscopic scale – either with single nanotubes or CNT networks.

[15] Carbon nanotubes have high thermal stability, thermal conductivity and usually reasonable electrical conductivity. [15] [16] However, chirality and the diameter play a decisive role on whether the nanotube is semiconducting or metallic – the sort that statistically one third of nanotubes are like whereas the rest are semiconducting [17]. As of today, nanotubes cannot be grown with a specific chirality [18], which is one of the major challenges limiting their use in practical semiconductor-based electronics. It is worth noting though that a few strategies exist for separating semiconducting and metallic SWCNTs. In one, metallic forms can be destroyed selectively by burning them off by passing large current through networks of mixed semiconducting and metallic nanotubes leaving mostly semiconducting ones intact. Another method is based on density gradient ultracentrifugation (DGU), which relies on separating solid matters dispersed in a density gradient medium such as iodixanol based on their densities. [19] [20]

There is a certain level of metal impurities in the commercial SWCNT products [21]. The amount of impurities in the SWCNTs used in this research is 5-7% according to manufacturer, which may have some effect on conductivity and account for some anomalies found in the images shown. Although the CNT itself is very strong, the networks of individual and bundled SWCNTs are held together only by van der Waals forces [14]. The networks created from these one-dimensional tubes are very flexible, however are subject to breaking when stretched extensively or repeatedly. [22]

MWCNTs are inferior compared to SWCNTs when it comes to electrical applications, since MWCNTs only conduct current in their outermost graphene layer, thus the presence of inner layers in the wall results in excessive cost of optical transparency or filler load in composites. [23] Pure CNTs are hydrophobic, thus disperse poorly in water and other usual solvents. This can be remedied for example by functionalizing them with polar surface groups (carboxylic, hydroxyl) that help their stabilization in polar solvents, or by applying surfactants [24].

2.1.2 CNT as a sensing material

Mechanical deformation changes the electrical conductivity of materials. Piezoresistive effect means that the resistance change of a material is not dependent only on the geometrical changes. Gauge factor is the ratio of relative change in resistance R_0 to the mechanical strain ε and can be calculated as,

$$\mathrm{GF} = \frac{\frac{\Delta R}{R_0}}{\varepsilon} = \frac{\frac{\Delta \rho}{\rho_0}}{\varepsilon} + 1 + 2\nu$$

where, ν = Poisson's ratio, ρ = resistivity, ΔR = change in resistance. For many materials, GF ~2, but for materials with piezoresistive properties, this can be many magnitudes higher. Having a strong piezoresistive property, sensors using CNTs have a good potential for sensing tiny deformations [25]. It has been established that CNT-based devices have good recoverability and reproducibility in cyclic loading tests. Though, when larger strains are applied, only part of the resistance will be recovered as the network will permanently deform and break. Stretching and contracting a CNT

network is also not a symmetrical process. It takes time for network to recover after being stressed. If the network strain direction is changed quickly enough to the other direction, network reformation and its resistance will be different between the two stages. [26]

2.2 Inkjet printing

Inkjet printing is an additive manufacturing process to achieve fast and relatively high-resolution patterns on many kinds of substrates without the need of e.g. photolithography or any other expensive equipment or cleanroom. Its versatility and relative ease of use makes it perfect for prototyping stages but also has a potential for larger scale manufacturing if set properly.

2.2.1 Inkjet printer

Dimatix materials printer DMP-2850 (Figure 1) was selected for the SWCNT ink deposition mainly because of its high resolution and accurate and repeatable placement of droplets up to 20 µm accuracy. It also is relatively cost efficient and easy to use. Piezoelectric nozzles have an orifice of 21.5 µm and they deposit 10 pL of ink per droplet. For optimal operation, Dimatix recommends that the orifice should be at least 100 times the particle size and the ink should be filtered through 0.2 µm filter if necessary. To help keep different inks separated the nozzles are not integrated part of the printer but a part of the cartridge. This property also makes the nozzles easily cleanable or replaceable when clogged. The reservoir is compatible with multiple solvents and substances associated with CNT and its capacity is only 1.5 mL to minimize the amount of expensive inks wasted.

Too big particle size contributes to nozzle blockages and increases the amount of cleaning cycles needed. Dimatix's software has three options for that. Blot that is used to wick excess ink from surface of the nozzle, spit that uses piezoelectric jetting to release ink from the nozzles as in printing, and purge that uses 5 psi (34 kPa) pressure difference to force the ink through the nozzles. Sometimes the nozzles of the cassettes were cleaned by soaking them in solvent and forcing pressurized air of up to 20 kPa through the cassette and nozzles. This however tends to break the silicon containing the nozzles, so it is only done as a last resort.

Dimatix DMP-2850 has many useful features regarding experimental type of printing. Drop spacing setting allows inkjet droplets to be spaced with a certain fixed intervals, layer setting controls the amount of layers of ink deposited and temperature control for platen and nozzles help control the viscosity of the inks and the drying effects on the substrate [27]. It also has some imperfections. For example, sometimes it is not possible, probably due to a bug, to print one drop wide patterns with the printer. To fix this, two parallel lines must be printed, other aligned to an irrelevant area.

Figure 1: Dimatix Materials printer DMP-2850

2.2.2 Inks and printing progress

Printable ink must meet certain standards to be able to jet through the tiny nozzles of the piezoelectric injection transducer. Dimatix even has its own guidelines and recommendations for the jettable fluid formulation, but some of the qualities will be hard, or even impossible to fulfill with solution used in our work. For example, the SWCNT used has a particle size bigger than the recommended 0.2 μm.

As the nature of the project of printing nanotubes with materials printer is hugely experimental, any unnecessary factors were sensible to be ignored and only concentrate on the significant factors such as printing performance and the pattern quality. Health concerns were considered only for handling the ink when preparing it and filling in the cartridges. Although the SWCNTs were expensive, the amount needed was very small and the costs were overshadowed by the cost of cartridges that were prone to blockages and even breakages when attempting to manually unblock them.

Pure CNTs are generally hard to disperse in water as they are highly hydrophobic, thus carboxylic acid functionalized single-wall carbon nanotubes (SWCNT-COOH) were used whose polar side groups can interact with polar solvents thus stabilizing the solid particles in the medium. Solid drying particles such as surfactants like SDS, although they could have been beneficial in terms of surface tension and possibly deter early CNT agglomeration, were avoided so that the finished product would have the least number of contaminants and particles to affect conductivity and other properties.

2.2.3 Printing effects and principles.

Coffee-ring effect is a well-documented phenomenon, in which a spherical droplet of liquid dispersion leaves a ring-like deposit after drying on a flat surface. At the edge of the droplet, evaporation happens faster resulting in a radial flow of the solution outwards from the center thus carrying more dispersed particles to the perimeter. Since

for many surface-solvent systems the edge of the droplet is pinned at the perimeter, after drying, most of the solid content of the dispersion deposits along the rim. [28]. In inkjet printing, this phenomenon is in effect especially with slowly drying inks and hydrophobic surfaces. Here, both conditions are fulfilled making the effect particularly existent.

There are also many effects related to the working of the inkjet printer that may not have been documented before. Many of them, such as band wandering and splattering, are related to blockages or partial blockages of the nozzle which impair the printing performance. Band wandering is the phenomenon of vertically printed bands wandering in horizontal direction tens of micrometers from assumed printing location. This happens due to partial clogging of the nozzle making drops fire diagonally making prints less uniform, wider and less repeatable. This can be remedied by frequent monitoring of droplet forming through the drop watcher and using inks that are less likely to clog the nozzles. Splattering is an effect when a nozzle is about to get clogged and thus starts firing sub-optimally. Namely, a part of the droplet breaks off and shoots somewhere to the side thus decreasing print quality.

Accuracy of the placement of the droplets is affected by changing jetting velocity of the droplets while the cartridge containing the nozzles maintains a constant velocity. When the carriage has a velocity of 0.07 m/s and average distance of 500 µm between the nozzle and the substrate, it can be calculated that with a 4 m/s drop velocity that equates to a drop drift of 9 µm, and with a 7 m/s drop velocity, to a drift of 5 µm. This creates up to 4 µm difference for the landing spots of the droplets. In this work however, the effect of this phenomenon is almost negligible and in all printing cases, it was enough that the droplet velocity was adjusted to this 4-7 m/s range with the help of the drop watcher and checked regularly.

To take these effects into account and to avoid blockages and other inconsistencies during printing, before printing it was ensured that the drop jetting angle is as perpendicular to the nozzle surface as possible and that there are only singular droplets jetting – no droplets separating from the tail of the droplet and re-joining the main droplet even in the beginning. Also, the relative velocity to other nozzles were compared. Similar velocity not only minimizes the jetting lag but it also tells about the nozzles having similar composition – probably having no contaminants inside them. Droplet size was also visually inspected to be as big as possible as it is affiliated to an unclogged and clean nozzle.

2.2.3.1 Dimatix reference parameters for the ink formulation

Dimatix recommends the solvent of the fluid to be of a low evaporation rate to avoid drying of the ink in the nozzle. Viscosity is preferable to be between 10 and 12 cPs (10-12 mPa·s) at the operating temperature while the printing head can be heated up to 70 ºC to lower the working viscosity if necessary. Although fluids having lower viscosity can be jetted, the operating performance is typically limited. Viscosities up to 30 cPs (30 mPa·s) at jetting temperature are said to have been jetted while drop velocities may be too slow for some applications. Surface tension should be between 28 and 33 dynes/cm (0.028-0.033 N/m) and surfactants can be used with water-based fluids to achieve this surface tension range. Again, high surface tension fluids up to 70

dynes/cm (0.07 N/m) may be jetted with limited performance. Particles dispersed in the ink must not settle or agglomerate rapidly, and removal of any dissolved gas is recommended especially for water-based fluids. It is said to improve jetting and priming characteristics of most fluids. pH for the ink is recommended to be between 4 and 9 for it to not cause corrosion and damage to the cassette and the nozzles. [29]

2.2.3.2 Ink formulation and printing progress

Even though inkjet-printing is a straightforward process at the first glimpse, getting many critical characteristics, such as the ink parameters, printer settings such as temperatures and jetting velocities so that a pattern of good quality can be consistently produced, requires a quite amount of effort. This part explains the multiple iterations and experiments with different kind of substrates and ink options needed to be done to achieve the desired ultimate patterns in the end.

First, the printer settings were dialed in with Dimatix's own model ink to get familiar with the general use of the device. The first leftover SWCNT dispersion from Ronja Valasma's Bachelor thesis containing dilute ammonia solution as the solvent for 0.02 mg/ml of carbon nanotubes, named SWCNT 1.0, was examined to be used with the printer. It was discovered that the solution must be properly dispersed with at least not big visible particles floating to avoid blocking. Fortunately, the dispersion did not have to be filtered with a 0.2 µm filter, which would have removed most of the CNTs but needed to be centrifuged to get rid of the big agglomerates. In addition, sonication with an ultrasonic cleaner was used to break down clumped agglomerated particles for the best results. Here, the criterion of the particle size being under 1/100 of the orifice could not be fulfilled as the size of the SWCNTs used in all the inks used is as much as 4-5 nm × 0.5–1.5 µm (Sigma-Aldrich 652490-250MG). In practice though, the blockages happened mostly when the cartridges were let dry while exposed to air either in the machine or on the shelf. Good enough operation was achieved when the printer was kept in a continuous use. The pH criterion of 4-9 was achieved with all the inks formulated and used in this thesis.

SWCNT 1.0 was printed on different types of substrates to examine surface effects: paper, alumina, PET and a self-made PDMS film (Sylgard 184). This ink, if properly dispersed and filtered was quite transparent and suitable for printing somewhat conductive but also heavily coffee-ringed pattern, with sheet resistance in range of tens of kΩ/square with 50 layers and 5 µm drop spacing.

To make printing easier and faster, a more concentrated SWCNT 2.0 was made using butanediol and water to disperse 0.08 mg/ml of CNTs so that conductivity could be achieved with fewer number of layers. This ink was noticeably more concentrated already and had a good consistency, viscosity and surface tension for jetting from the nozzles. However, unexpected jetting difficulties arose when trying to print with higher nozzle temperatures than about 35°C probably due to gas bubbles forming inside the nozzle when the ink warmed up. It also dried very slowly due to butanediol having a low vapour pressure at such temperature. It was still good for many, almost transparent prints in certain situations but was soon replaced with SWCNT 3.0 – a dispersion with a significantly higher CNT concentration of 0.316 mg/ml dispersed in

a 50 wt.% DMF and 50 wt.% water solution. The parameters of these three different SWCNT-inks used in the research are compared in Table 1 and the visual aspect in Figure 2.

The self-made PDMS was attempted to treat with APTMS (diluted in hexane) to achieve higher hydrophilicity. The surface became very milky and tended to wrinkle because of the hexane content in the solvent. Although the surface changed considerably to the naked eye, the contact angle did not change and thus this method was abandoned. Later we decided to use argon-plasma treatment that had been proved to make visibly transparent hydrophilic surface in previous studies.

SWCNT 3.0 was formulated to have a highly concentrated but still fully dispersed CNT ink. DMF as a polar solvent offers SWCNT concentrations of 1.0 mg/ml as opposed to waters 0.1 mg/ml. It was used to help disperse SWCNTs alongside water which has a higher vapor pressure aiding drying. DMFs and waters viscosities are both close to 1 mPa·s, so the final viscosity was known to become lower than recommended. Also while the surface tension of pure DMF in 20 °C is almost ideal at 0.0371 N/m, the higher value of water at 0.0728 N/m can be exploited to counter too low viscosity somewhat as it holds the meniscus better in the nozzle orifice [30]. These qualities did not become deciding factors however, as the printer was known to be able to print even pure water-based inks with very high surface tensions.

Water already has so high vapour pressure that it is considered as a quickly drying solvent in inkjet printing. With a 50/50 wt.% DMF and water blend was achieved a lower boiling point and higher concentration while still maintaining good enough viscosity and surface tension. This allowed for faster printing because of faster drying solving some of the issues with ink droplet merging together and travelling on hydrophobic surfaces that are induced by slow drying. The enabled high concentration of dispersed SWCNTs also helped printing well-conductive films with significantly less numbers of repetitions than with the other inks. This solution may expire over time though, as DMF is known to hydrolyse into dimethylformamide and formic acid in a water solution. SWCNTs used also have a 5-8% metal content, which are likely catalyst transition metals, such as iron, that can also catalyse the reaction of DMF into other compounds [31]. This was considered by printing the ink as soon as possible after the blending and by visually inspecting it periodically.

Two-dimensional printing patterns were examined and proved possible, but since the best quality prints had been achieved for one-dimensional lines, we settled for those although the process was slower.

When we started printing on the PDMS-films provided by VTT, patterns were easier to see on it as the surface was very smooth. This both helped the process but also challenged it with more prevalent drying issues and ink traveling phenomena on the surface. Luckily, these effects were prepared for as PDMS has been long known to be very hydrophobic and an exploration to a surface treatment with argon plasma followed. This process allowed for various performance improvements when the treatment times and other factors were tuned in carefully - explained in a greater detail in chapter 2.3.1. Soon after this stage the SEM images were taken with various platinum metallization settings. This was followed by a new batch of SWCNT 3.0 which was made with all other properties, such as concentration, viscosity and surface tension identical to the previous one with the only difference being 20 minutes of more

sonication. All prints in this thesis are done with the original SWCNT 3.0 or this practically identical re-batch.

A Finnsonic M12 200w/800w ultrasonic device was used to help CNT dispersion and to separate dissolved gases from the dispersion. The centrifuge used was a Hettich Zentrifugen universal 320 at 3500 rpm for 10 minutes at a time. The SWCNT 3.0 concentration was measured by evaporating the precipitate left over from ink formulation solvent in a good ventilation and weighing the amount of CNT left in the tray. This was also compared to a small sample of evaporated ink and the results were similar within a margin of error.

Table 1: Comparison of the different SWCNT-inks used in the research.

	SWCNT 1.0	SWCNT 2.0	SWCNT 3.0
Composition	300 ml H_2O Distilled 3 mL NH_4OH 10.8 mg SWCNT-COOH (Sigma-Aldrich 652490-250MG)	21.44 g H_2O 6.95 g 2,3 -Butanediol 2.27 mg SWCNT-COOH (Sigma-Aldrich 652490-250MG)	13.05 g H_2O Distilled 13.06 g DMF 13.1 mg SWCNT-COOH (Sigma-Aldrich 652490-250MG)
Processing	3h sonication 30 min centrifugation Supernatant collected	60 min sonication 4 times 10min centrifugation and supernatant collection. Lot of the CNTs present in the precipitate.	2 min magnetic mixing 30 min sonication in 50C 4 times 10min centrifugation and supernatant collection.
Color	Light amber	Dark amber	Almost opaque black
Water %	99	76	50
Butanediol %	0	24	0
DMF %	0	0	50
CNT calculated (mg/ml)	0.036	0.08	0.5
CNT measured (mg/ml)	0.02 ± 0.003	-	0.316 ± 0.017
pH	9	6	6
Note	Ink from Ronja Valasma's work. [32]	First fully self-formulated ink.	Final ink used in all the prints in this work.

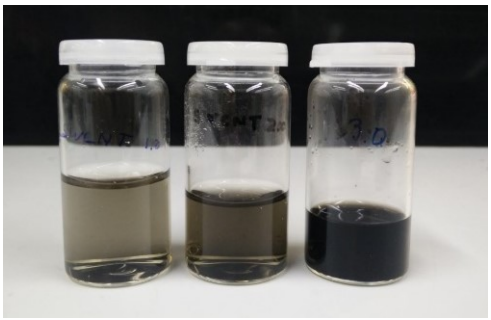

Figure 2: The three SWCNT inks used in the research in order from left to right.

2.2.3.3 Ink degassing

Piezoelectric jetting relies on pressure change in the nozzles forcing the fluid to jet out of the orifice and pump new ink to the nozzle from the reservoir. Gas can appear in the print nozzles from two sources. Atmospheric air bubbles and dissolved gases forming bubbles through a process called rectified diffusion. Atmospheric air bubbles can be bled out by purging and using cleaning cycles, but dissolved gases require other methods. As Dimatix materials printer does not have a degassing or vacuuming system, degassing must be done before injecting the liquid into the reservoir if bubble forming ends up being a problem [33] [29]. The effect of rectified diffusion can also be of benefit when degassing the ink with an ultrasonic bath. Sonicating the fluid makes dissolved gases form bubbles and float out of the dispersion [34]. This was the main method of degassing inks discussed in this work. Degassing can also be achieved in a high vacuum or by heating the liquid close to its boiling temperature [33].

As a practical example in our work with an ink that contained mostly water and some butanediol, jetting problems were encountered only when nozzle was heated, which further incites bubbles formation. Heating and sonicating the ink provided only short remedy for this issue and problems returned shortly after the cartridge had cooled down. This was fixed by using SWCNT 3.0 solution only which was free of the phenomenon.

2.2.4 Printing time with Dimatix printer for small patterns.

Dimatix printer works by moving the printing head horizontally from left to right and jetting droplets in defined spots which is similar to most commercial inkjet printers. Between vertical bands, platen is moved in y -dimension, i.e. vertically, to print the next horizontal lines. This cycle takes approximately 2.2 seconds. Thus, printing lines horizontally is noticeably faster than vertically. With vertical patterns, line length is equal to print height, and is directly proportional to the printing time. With horizontal patterns, it is possible to achieve fast printing as ceiling function component ceil(Ph/DS) becomes one, and the total time is consequently dependent mostly on the layer count. However, with hydrophobic surfaces and slowly drying inks, printing must be done vertically or horizontally through multiple prints as drops cannot be placed touching one another because of droplets joining together. For small patterns, the drying time between drops is the time that one horizontal pass takes, i.e. 2.2 s, and compulsory cleaning time between layers, 7 s in the minimum. Therefore, total printing time in seconds is

$$\mathrm{Tprint} = \mathrm{LC}(\mathrm{DT} + 7 + 2.2\lceil\frac{Ph}{DS}\rceil)$$

where print height is Ph and drop spacing is DS in the same unit of distance, layer count is LC and extra drying time or waiting time between layers in seconds is DT. For example, for a vertically printed line with a usual layer count of 20, print height of 1000 µm and drop spacing of 20 µm, total time is 2340 seconds = 39 minutes.

2.2.5 Printing methods for hydrophobic surfaces

Printing CNT to a completely untreated PDMS surface is appealing due to its simplicity, speed and because it requires little expensive machinery. Extremely hydrophobic surfaces, however, present challenges to printing with the droplet not spreading evenly to the surface to dry or even absorbing into some less hydrophobic materials on the surface, such as ink that has dried previously.

If a new droplet is placed too near or touching an existing non-dried droplet on a very hydrophobic surface, the droplets merge and travel to the direction of printing leaving uneven or no printed pattern at all. This creates confusing patterns that only have globs of ink throughout the expected printing area or only in the end and inconsistent gaps in between and as a result, printing resolution suffers greatly. It is also possible for the new droplets to become absorbed on the previously dried ink – CNT or silver, which are far more hydrophilic than the untreated substrate.

Horizontal lines are considerably faster to print but drying time between the droplets is only microseconds, which makes drying of the ink, or lack of, challenging. In case of hydrophobic surfaces, change of method is required. Another possible method is to print with a large drop spacing to leave gaps in between droplets and to later print in these gaps. Dimatix Drop Manager does not internally have an official, repeatable way to change the droplet locations to print in between the droplets because they are tied to a grid, whose dimensions are determined by the drop spacing. It can only be done manually using a fiducial camera by moving the print origin instead that moves the grid as well. Repeatable, good quality patterns need more research to be done with this method as it is still subject to ink absorbing issues and not to forget the large amount of manual adjustment needed due to the limitation of the software. Good results should still be achievable with higher layer counts and the help of argon-plasma treatment though. This method gives the highest drying times between the droplets and it can even be adjusted by waiting between the prints just in case, and it has the potential to be much faster than printing droplets vertically one at a time.

These vertically printed lines of droplets have a non-changeable ~2.2 s drying time between adjacent droplets giving repeatable and robust although slow printing throughput. Adjacent vertical patterns have been attempted too, but the quality suffers because of newly deposited droplets getting sucked into the existing dried or partially dried ones without very careful choice of settings. Printing only one vertical line at a time gave us the most robust and repeatable results for this work allowing for long enough drying times with reasonable amount of manual adjustment.

2.3 Substrate material

The substrate material is a silver screen-printed PDMS film made by VTT (Figure 3 A). The PDMS used is Wacker ELASTOSIL Film 2030 and the ink is Creative Materials 125-19FS. It consists of 95 µm thick PET-backing film (non-stretchable support), 100 µm PDMS elastomer, and a patterned silver ink, whose thickness is about 7 µm for single layer and 15 µm for two overlapping layers. The sheet resistance of the silver pattern varies from 0.15 to 0.27 Ω/sq. [1]

To prepare the substrates for printing, they were cut into 10 mm by 25-50 mm pieces using scissors. There were two main types of samples used in this work. The first type, shown in Figure 3 B, was the original substrate split in two lengthwise so that the pads were separated electrically to achieve 1 mm wide gap to fill with the CNT line pattern. The PET backing was left in place to ease the handling and to protect the membrane from stretching.

In stretch, pressure, gauge factor and heartbeat measurement tests, the PDMS film was used without splitting so that the silver could be used as a contact pad, shown in Figure 3 C. Silver track was manually removed from one spot to separate the paths electrically and in the adjacent 1 mm gap, the SWCNT track was printed. PET support was first used with the same reasons as with the electrical measurements but later it was removed to enable the analysis of elastic properties.

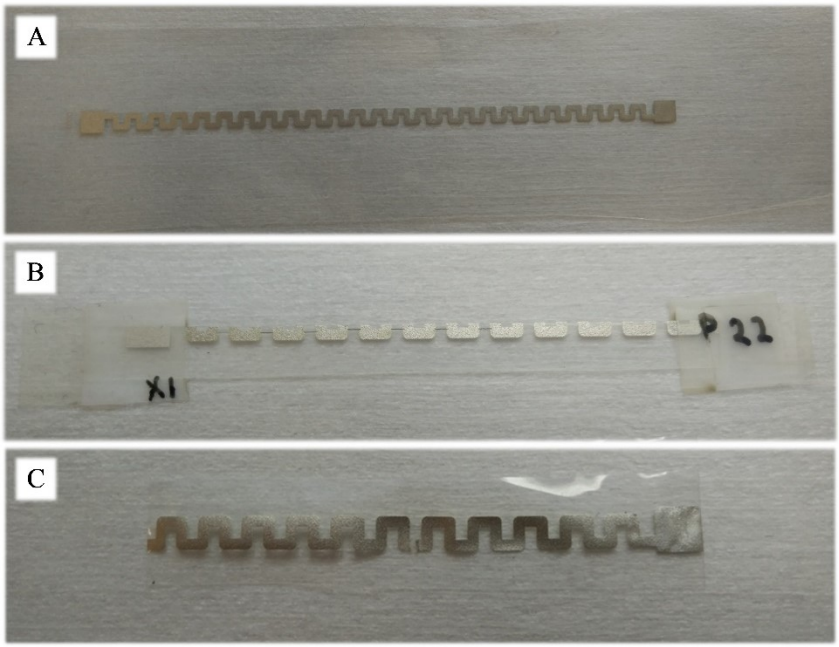

Figure 3: **(A)** The original screen-printed sample received from VTT. **(B)** The sample type used for general electrical measurements. **(C)** The type used for stretch- and sensor measurements.

2.3.1 Treating PDMS with argon-plasma

Argon-plasma treatment has been proven useful for treating polymer-based substrates to become hydrophilic [35]. It was chosen for this work too due to earlier successful experiences with treating polymers, such as PET, in making them more hydrophilic as well as that the process was already well known in the Microelectronic Research Unit. Also, oxygen-plasma was speculated to possibly etch or oxidize the silver ink present on the PDMS. The cut PDMS samples were taped on a silicon sample holder used in the Oxford PlasmaLab Plus (Figure 4) plasma etcher. 200 W plasma power was applied and the argon flow was set 20 sccm at a pressure of 20 mTorr. Treating times were checked from 2 to 30 min. Too short times made the PDMS to have a good enough hydrophilicity at first, however it faded faster than with longer treatment

periods leaving not enough time for printing. On the other hand, too long treatments resulted in excellent although non-uniform hydrophilicity. Especially around the printed silver conductive paths, problems arose during printing as ink repelled the PDMS in the interface area and started to wet the silver too well instead. This could have happened because plasma affected the silver more aggressively than the nearby PDMS thus creating a hydrophilicity gradient too steep at the interface. A treatment time of 13 minutes combined with a 5 to 10 hours of waiting after the treatment before printing gave the best overall result and was chosen to be used in all the samples in the electrical measurements.

Figure 4: Oxford Plasmalab 80 Plus.

Figure 5 shows AFM surface topology scans of treated and untreated PDMS surfaces at different magnifications. Treatment is 10 minutes long argon-Plasma at 200 W power. On the surface of the original PDMS, 100-200 nm deep cracks can be seen that deepen during the treatment. Zoomed between the large cracks, the untreated surface is smooth, having only 2-6 nm high bumps, whereas the argon plasma treatment makes the surface to have a fish scale-like appearance with up to 100 nm cracks and up to 100 nm high bulging nodules.

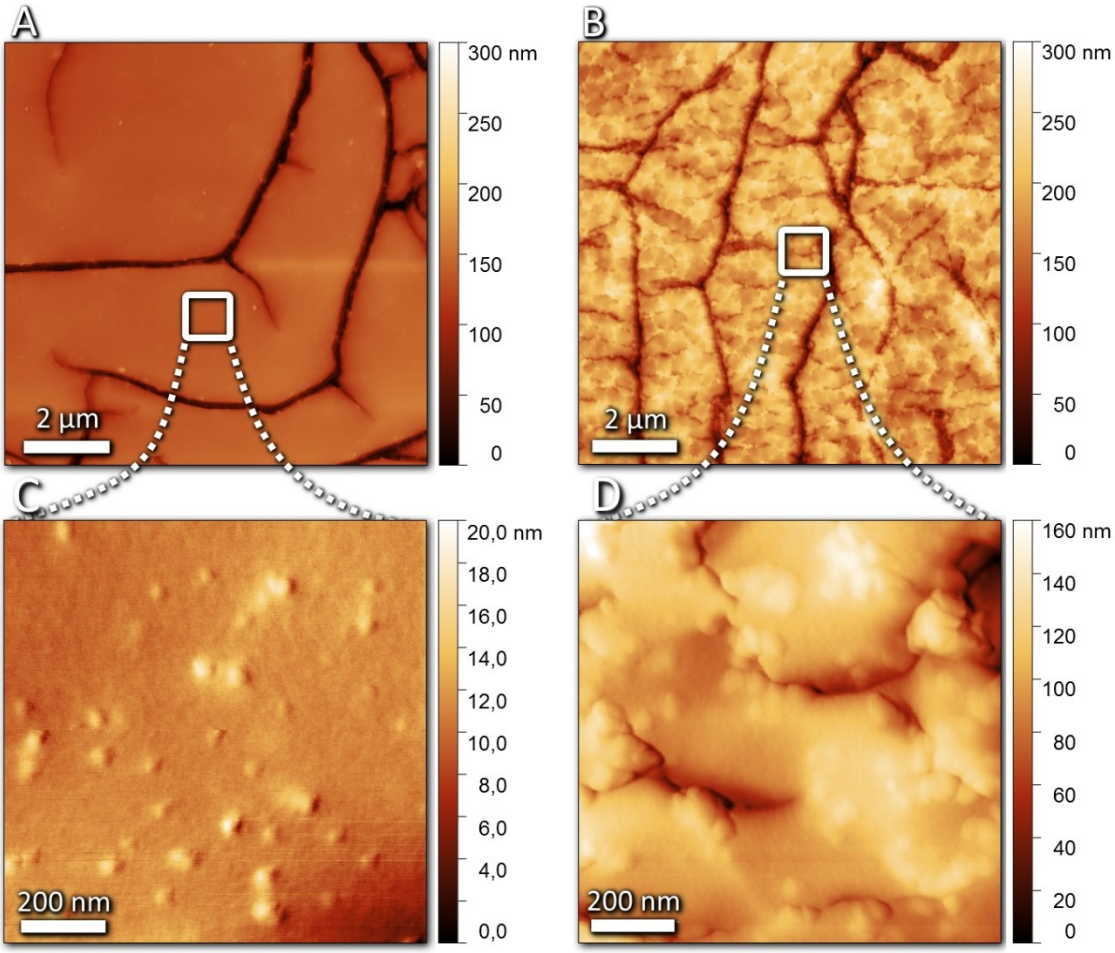

Figure 5: AFM topology images of a 10×10 µm and 1×1 µm area to compare **(A, C)** untreated and **(B, D)** treated PDMS surfaces.

2.3.2 Substrate transparency

UV-vis-NIR Varian Cary 500 spectrophotometer was used to determine the transparency of the substrates. PDMS and PET films are both clear to the naked eye, but the plasma-treated PDMS is a little bit opaquer due to light scattering on the surface. This is expected to make the difference in transparency between treated and untreated PDMS substrates, also apparent in Figure 6.

CNT tracks used in this work practically block incident light thus affecting the overall transparency. (The substrate transparency is decreased by the ratio of CNT coated footprint area and the total area.)

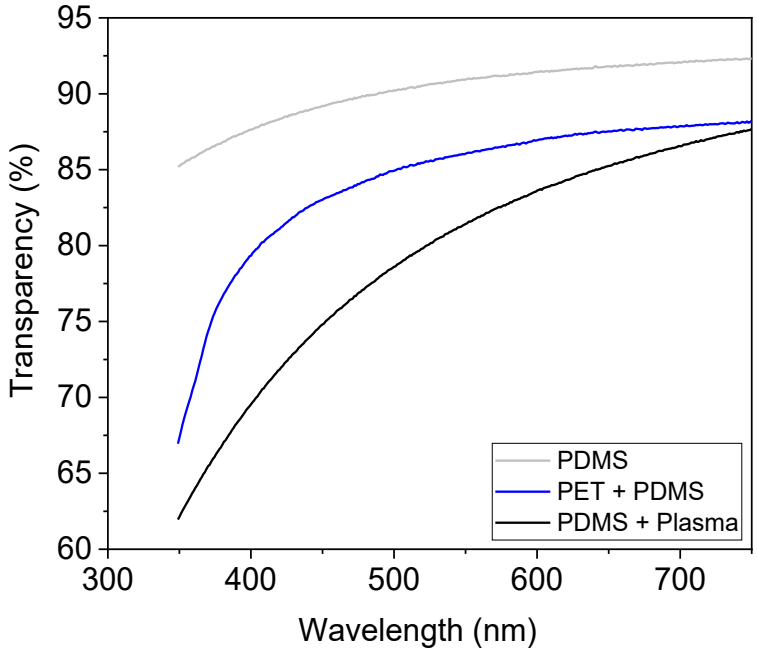

Figure 6: Comparison of transparencies of the substrates.

2.3.3 Contact angles

The contact angles are collected to the Table 2 below and the corresponding images from which the angles are measured, in Figure 7. The contact angle measurement shows great difference between treated and untreated surfaces, indicating a more hydrophilic surface and success in the treatment. Also, there are differences between DI water and SWCNT contact angles on both surfaces, SWCNT angles being systematically lower.

The angles are measured from their advancing stage, when the droplet and its angle is at its highest. Droplet diameter is about 7 mm. Pictures are taken with a Canon Powershot SX10 IS from 5-6 cm away. Contact angles are measured with ImageJ software angle measuring functionality.

Table 2: The contact angles of water and CNT on untreated and treated surfaces.

Contact angles (°)	DI Water	CNT
Untreated	94.6	84.9
Treated after 10h	30.0	15.0

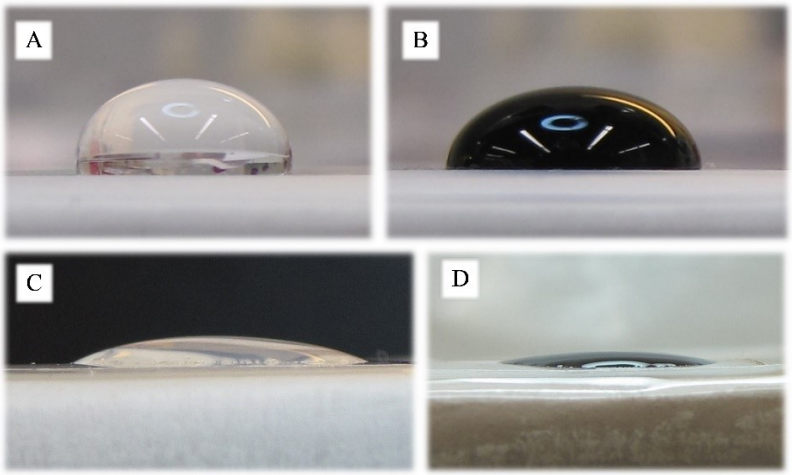

Figure 7: Surface wetting of plasma-treated and original PDMS. DI water on **(A)** untreated and **(B)** treated PDMS surface. SWCNT ink on **(B)** untreated and **(D)** treated PDMS.

2.4 Imaging equipment

FESEM, AFM and optical microscopy were used to visualize the microstructure of printed nanotube networks and silver contact pads as well as surface of PDMS substrates. First, high-resolution images were taken with Zeiss FESEM ultra plus (Figure 8 A). Surface charging is a serious problem with nonconductive materials, even with careful conductive carbon taping. Therefore, platinum coating was used to enable good grounding of the probing electron beam thus getting better image quality. Images were taken from three kinds of samples: with no platinum coating, with approximately 1.4 nm Pt coated layer, and with a 5 nm platinum coating on top of 1.4 nm coating for a total of 6.4 nm. The thicker the conductive layer, the less charging but also less details can be seen from the original material at the bottom due to the thick layer on top. The best image quality was achieved with 1.4 nm layer sputtered on the samples and that was used for the analysis here. Because SEM had limited resolution due to surface charging, AFM analysis was also performed using a Bruker Multimode AFM with μmasch NSC18 probes (Figure 8 B). Optical microscope pictures were taken with a camera through Wentworth probe station microscope (Figure 8 C).

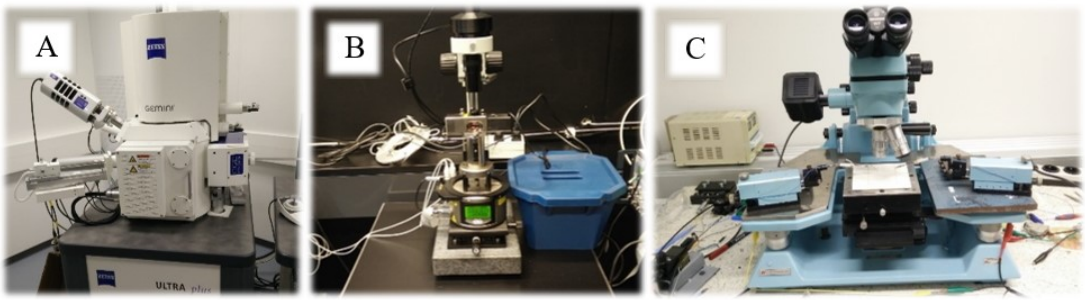

Figure 8: (A) Zeiss FESEM, **(B)** Bruker AFM and **(C)** optical microscope on a Wentworth probe station.

3 RESULTS AND DISCUSSION

To examine the printed micropatterns more closely, they were imaged, their conduction was measured and the use in strain and sensor applications was demonstrated with mechanical bending and stretching. On top of optical imaging, SEM was used to see the individual nanotubes and the interface of the CNT-pattern and silver, and AFM to figure out the exact height characteristics of the finished patterns.

Drop spacing was noticed to be a critical variable for achieving patterns with the best possible quality and layering the main factor to modify the conductivity. Both experiments were carried out by also comparing the effect of the surface treatment at the same time. Also, as the first droplets of a horizontal line are always more concentrated, this phenomenon was investigated as well. Multiple prints were executed for each set of settings and the results were averaged to rule out possible printing errors and other variations.

In the end, the tensile properties of micropatterns were studied by stretching them to find their pressure sensitivity and gauge factor. And they were also demonstrated as sensors for measuring bending and a human heartbeat.

3.1 SWCNT on PDMS

For electrical measurements, SWCNT ink was printed between the screen-printed silver pads so that the lines would have fixed length and that they could easily be measured without touching and damaging the CNT itself (Figure 9). SWCNT print was ensured to overlap the silver-coated surface for at least 100 µm for good adhesion and electrical conductivity.

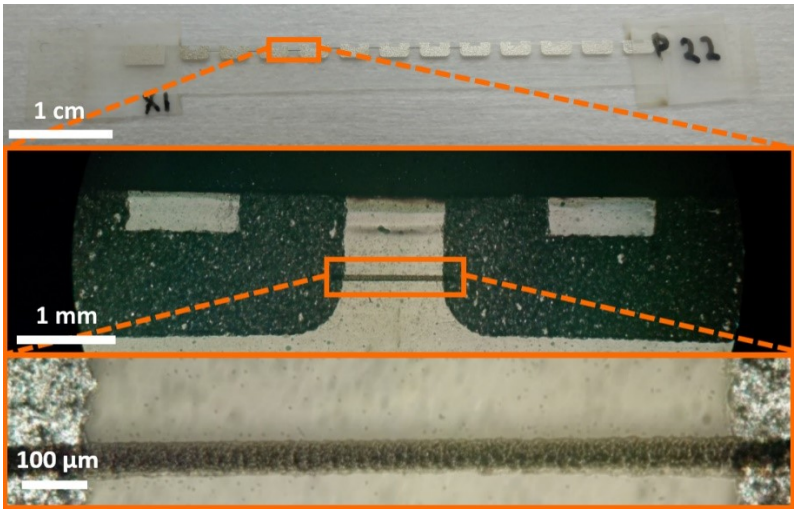

Figure 1: Inkjet-printed SWCNT line between silver pads with 15 printing layers and 20 µm drop spacing. Pad-to-pad spacing is 1 mm.

The thickness of the patterns depends on the amount of CNT deposited, which again is dependent on the number of the layers and drop spacing. Figure 10 shows the height profiles for a 12 layer, 10 µm drop spacing pattern, whose thickness is 1.5-1.6 µm, and for a single print pattern with 20 µm drop spacing having thickness of about 130 nm. In comparison, the single layer silver thickness is about 7 µm. Coffee-ring effect is the reason of thicker deposition in the edge.

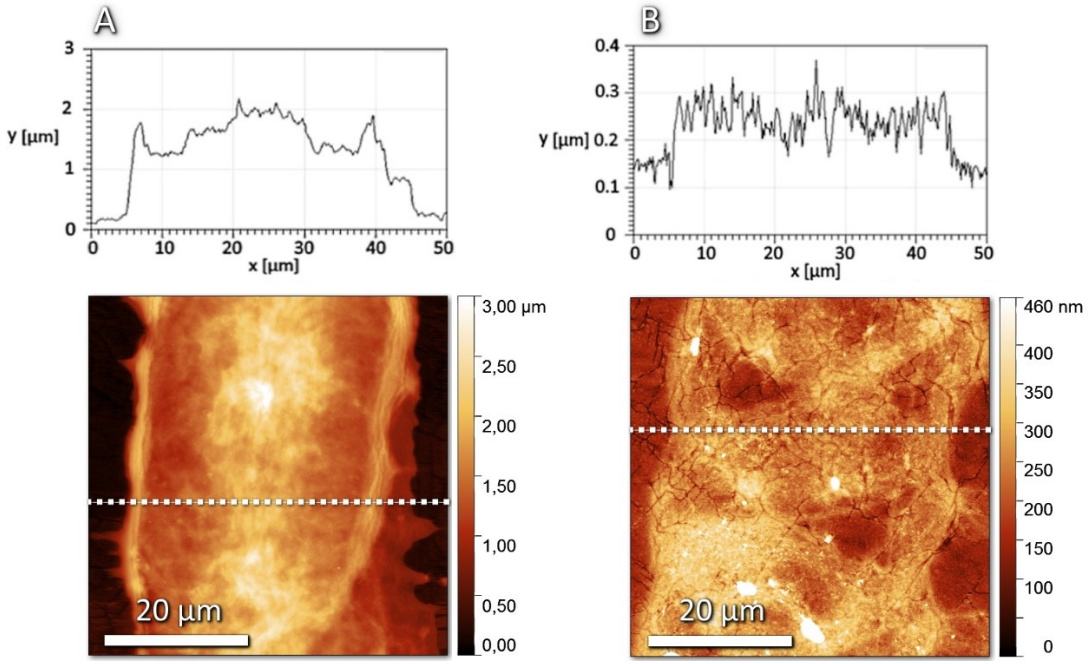

Figure 10: AFM topology scans for inkjet-printed SWCNTs on PDMS shows **(A)** 1.5-1.6 µm thickness for 12-layer patterns and the rim and centre of the structures, and **(B)** 130 nm thickness for single layer.

3.2 CNT on silver

SEM pictures from the interface of silver and SWCNT show how the ink has been absorbed between the silver flakes with a large surface area to achieve a very good adhesion. Figure 11 shows the silver flakes being about 2-15 µm in size, having micrometre-sized cracks and holes for the CNTs and networks to adhere.

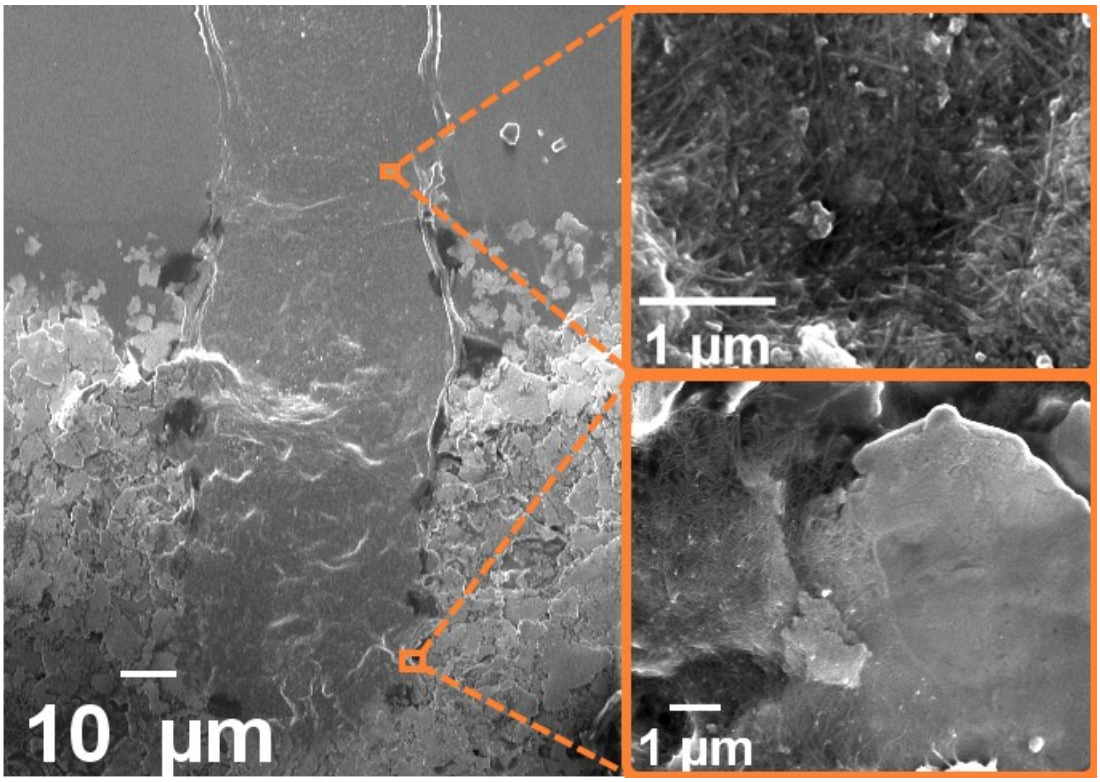

Figure 11: SEM images of a 15-layer SWCNT pattern on top of the PDMS and the silver pad interface.

3.3 Electrical probing

For the electrical measurements, samples were placed under the microscope on the Wentworth probe station and the probe tips were securely brought in contact with the Ag pads using enough force to minimize the contact resistance (without puncturing the pads). Done this way, the silver pattern, contact resistance and other series resistances combined were negligible combined to the resistance of the CNT pattern. All the following sheet resistances are calculated from measured resistances considering a mean track width of 46.3 µm and a length of 1000 µm. This track width was obtained from the drop spacing test samples, where also the standard deviation was 5.8 µm.

For the real-time resistance measurements while deforming the samples, a Keithley 2636A with an automated LabVIEW script was used to sweep voltages from -2 V to +2 V with a current limit of 1 mA to preserve samples, hysteresis enabled, 0.1 V voltage step and 100 ms delay in between the samples. The measurement device was attached via a BNC plug to crocodile clip leads into needles on the substrate.

3.3.1 First drop phenomenon

The first droplet of one horizontal line of droplets produces darker and more conducting patterns than the latter ones, making the leftmost vertical lines, the ones that were used in the electrical measurements in this work, more conductive than the

others. This happens most probably due to a more concentrated first droplet as there is no designed mechanism to change the droplet size other than partial blockages, which only make the droplets smaller. A more concentrated first droplet can happen when the surface of the droplet continuously dries in the nozzle and mixes into the nozzle due to idle meniscus vibration feature that keeps the nozzle unblocked. This behaviour was observed by printing 4 vertical lines with 10 mm intervals. The test was repeated 3 times. The electrical sheet resistances together with the mean values and their corresponding I-V curves are plotted in Figure 12.

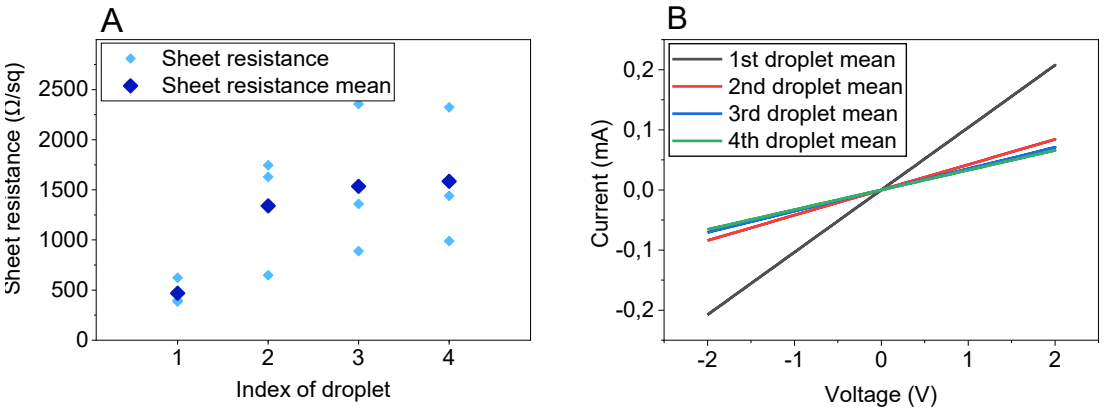

Figure 12: Nozzles idling effect on **(A)** sheet resistance and **(B)** their corresponding I-V curves.

3.3.2 Drop spacing effect on resistance

Drop spacing tests were carried out as similarly as possible on both plasma-treated and original surfaces. Through the adjustment of the number of layers printed, the amount of CNT deposited was standardized in the 1000 µm long gap between the conducting silver pads. Excluding the parts of the CNT track that overlapped the silver pad, the line consisted of 803-827 of 10 pL droplets (SWCNT 3.0 ink). Printing for treated surfaces was started from the 40 µm spacing specimen after 4 hours the treatment and ended with 5 µm spacing one after 10 hours.

The results, graphed in Figure 13, show that the largest drop spacing to achieve a conductive, uniform pattern is less than 40 µm. This was expected as the individual droplet size on substrate is usually between 35 and 50 µm. The best results were achieved with a 20-25 µm drop spacing. A 20 µm drop spacing was selected to be used in further resistance tests because of low resistance, consistency when printing and visually convincing pattern and quality among the best prints. Also, the amount of CNT deposited is easier to manage with layering when drop spacing is not very low.

On Ar plasma-treated surfaces the resistance of the printouts was significantly lowered (Fig. 14). Only low drop spacings of 5 µm had problem with drying with the used ink and settings making the track nonconducting in the treated case. 5 µm drop spacing gave surprisingly low resistance on untreated surface even though visually print quality was not excellent. Print quality varied a lot on the lowest drop spacings due to drying issues of droplets, which might affect the result.

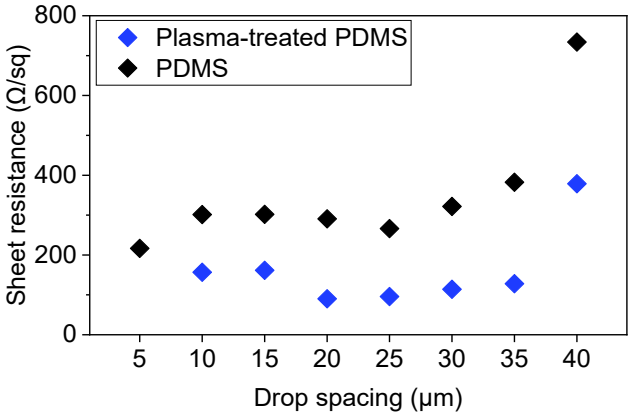

Figure 13: The effect of drop spacing on sheet resistance of printed SWCNTs on the surface of PDMS.

Overall, I-V curves of the drop spacing test patterns, in Figure 14, show linear (Ohmic) transport behaviour. With the drop spacing of 10-35 µm, the resistances were quite consistent. Only when the extreme spacing values applied, i.e. 5 µm and 40 µm, the results scattered from the trends of the data set.

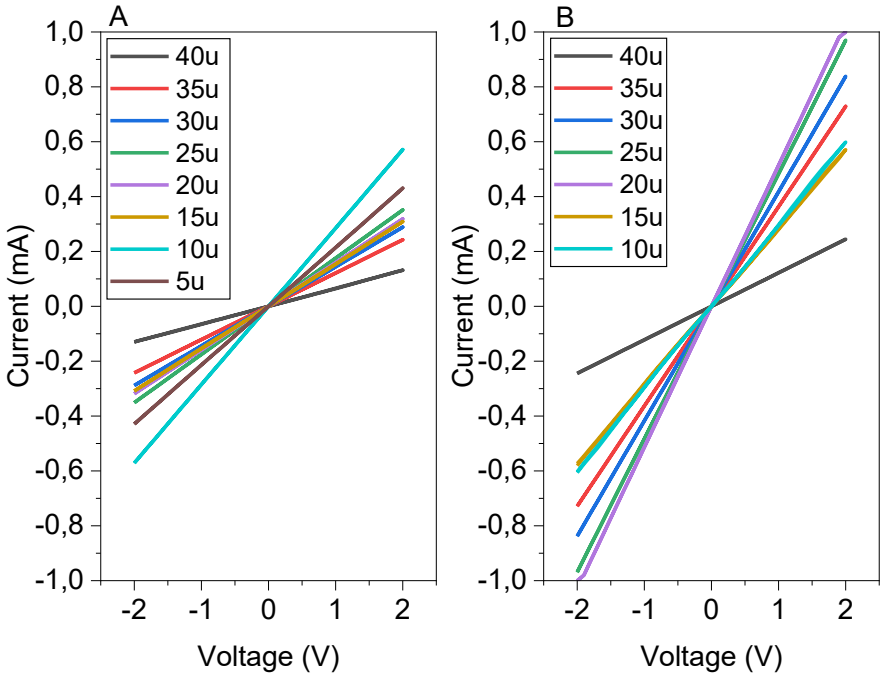

Figure 14: The effect of drop spacing and surface treatment on the I-V characteristics of printed SWCNTs on **(A)** untreated and **(B)** treated PDMS.

3.3.3 CNT Layering effect on resistance

Because the effect of plasma treatment reverts relatively quickly, prints were done in a successive manner while keeping the amount of time deviation as low as possible.

All prints were done in order starting from the least layers proceeding towards higher layer prints that also take more time. This was done to decrease unnecessary deviation between prints with the same number of layers, especially when it was avoidable with faster, lower layer count prints.

In a research on SWCNT printing on cloth fabrics and flexible substrates, the lowest resistance achieved was 78 Ω/sq with 200 layers [36] and in similar prints done to paper, best results were 760 Ω/sq with 12 layers [37]. Our average resistances achieved with 20 layers were 65 Ω/sq on treated surfaces and 243 Ω/sq on original, untreated surfaces which is already a better conductance per layer of material and lower overall resistance. Only with the treated surface, a conducting 1-layer line was possible to create. It had an average resistance of 7100 Ω/sq. Also, with higher layer count, substantially lower resistances were possible to achieve compared to the untreated substrates. The resistances of the same layer count are also lower in all treated samples (Figure 15). The same behaviour can also be seen in the I-V graphs (Figure 16).

Deviation of the resistance in prints increase greatly when the number of layers decreases because the drop spacing naturally makes the lines have a slightly uneven shape in the beginning. Successive layering decreases this effect or even fixes previous printing artefacts. With over 15 layers, both treated and untreated surfaces start to provide under 20% variation in the resistance - treated surface having the edge in this aspect too. Overall, the treated surface provides higher range of printable resistances making the process, although a bit more complicated, also a more versatile option.

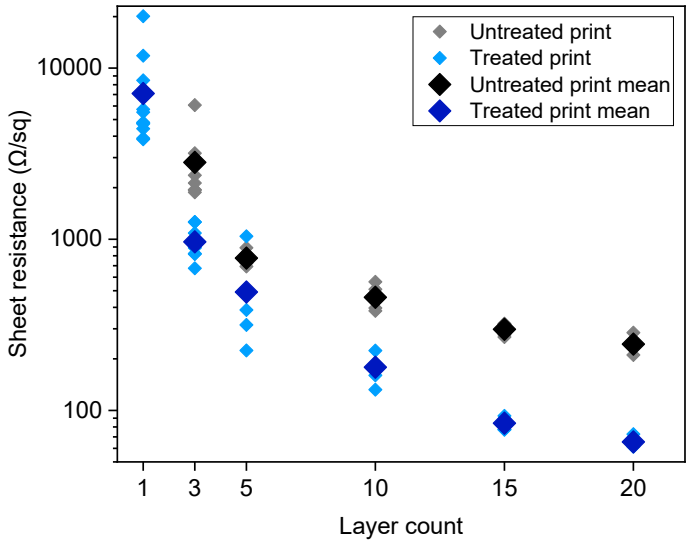

Figure 15: Sheet resistance vs. layer count and surface treatment.

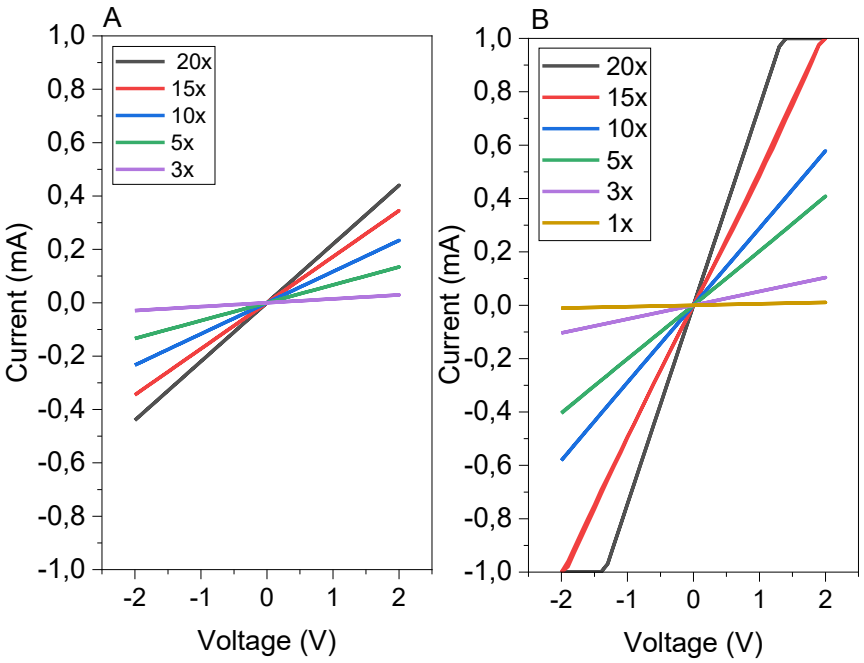

Figure 16: I-V characteristics vs. layer count on **(A)** untreated and **(B)** treated surfaces.

In Figure 17, a Belehradek power function $y = a(x - b)^c$ fit is presented to analyse the relationship of sheet resistance and layer count along with logarithmic scales. The treated surface is seen to conform to the fit of for percolating networks, and help obtaining the the percolation threshold (b) and the character of percolation with the power exponent (c) being -1.27±0.07. Accordingly, the results for the patterns printed on the plasma-treated surfaces are in good agreement with the percolation theory that expect power exponent of -1.33 for the resistance-thickness plots.

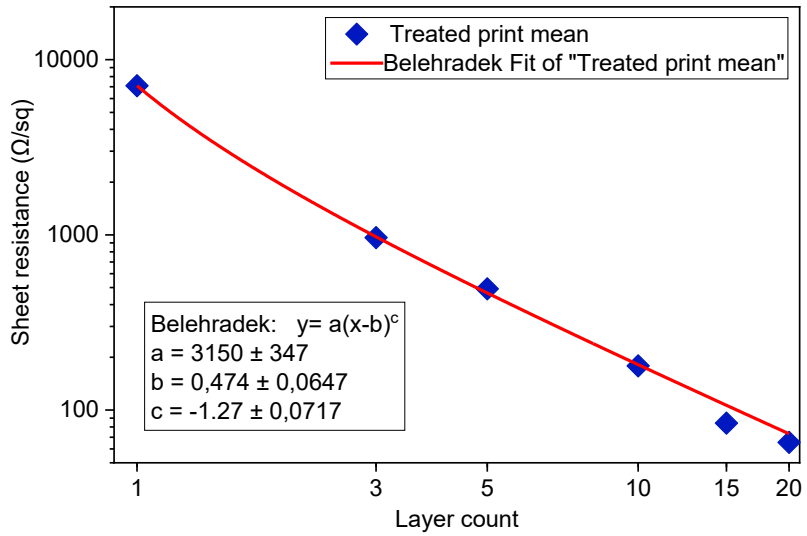

Figure 17: Belehradek-type power-function fit.

Because of the nature of CNT bundling and forming random connections, more layers give a higher chance of loose connections being connected resulting in lower resistance per layer or better conductivity for CNT deposited. In figure 18, the resistances are normalized to the amount of CNT deposited by multiplying the resistance with the number of layers printed, the effect of resistance lowering with increasing number of layers can be seen more easily. That is especially noticeable with treated substrate indicating it allows more efficient use of CNTs.

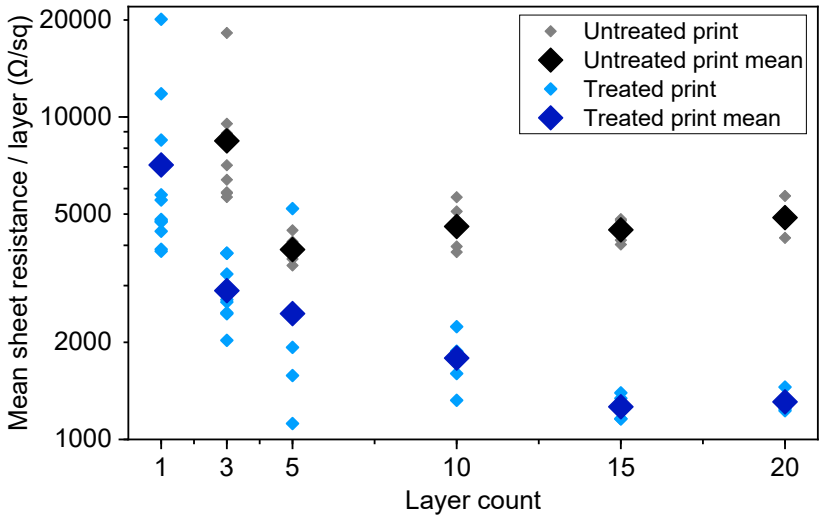

Figure 18: Mean sheet resistance per layer, the amount of CNT deposited normalized.

3.4 Tensile properties

For the stretching tests, we used a Linkam TST 350E stretch stage with a Linkam T95-PE controller. It has a positional resolution of 10 µm, which is feasible for our sample size and outputs data into a convenient format. For the real-time resistance measurement, Keithley 2636A with an automated Labview script was used. The setup was confirmed to give accurate resistance and current/voltage measurements up to 43 samples/s as 23 ms is the minimum step delay in the resistance range of 20-300 kΩ. The two measurement devices were scripted to be started and ended at the same time and the results were afterwards scaled to the same time domain. Gauge factor was later derived from the strain curves in Origin Pro 2019b.

Tentative tests showed that 3-4% of deformation was possible before permanently changing the resistance of the samples. Maximum strain and durability of the device was found to be comparable to other CNT based devices [26]. Multiple tests were conducted to achieve a noise-free, repeatable and reliable measurement setup for stretch testing. These first iterations included the use of the original PET-backing as a support for the PDMS so that the CNT on the very flexible membrane would not change its properties. For the measurements however, the PET backing and PDMS film was separated carefully from each other by sliding an oiled thread between them when the PDMS film was already securely attached to the stretching device from the PDMS film.

Many attachment options to the stretch stage were attempted including making the contacts from carbon tape, silver ink and or copper tape with its tape side down touching the silver path. All of them proved to be not conductive or reliable enough. The best method is shown in Figure 19. With the help of copper tape, Kapton tape and Linkam stretching device, a PDMS film containing screen-printed silver ink and CNT was stretched and analysed.

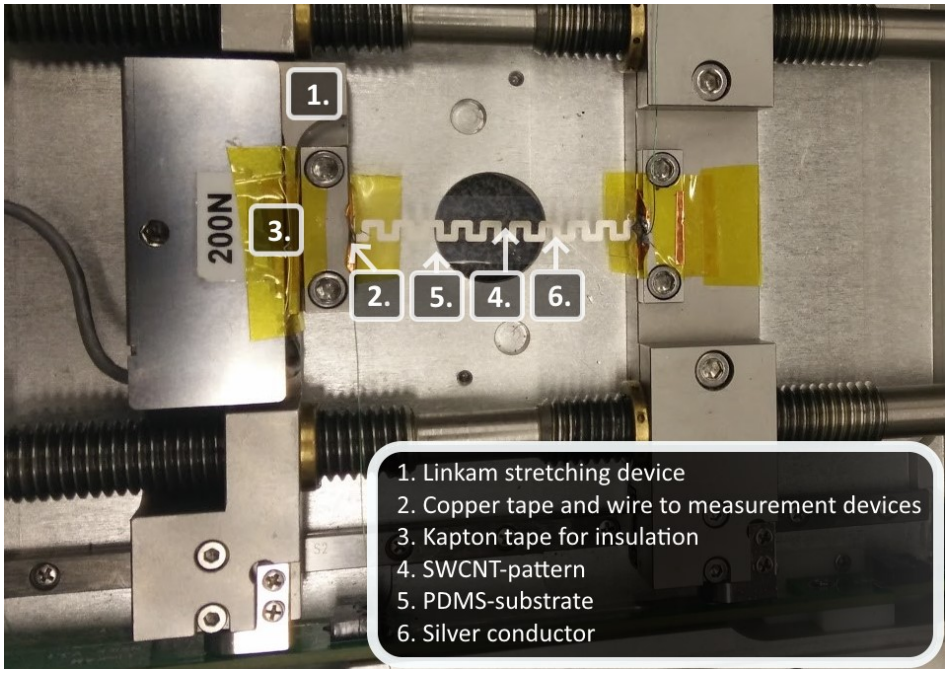

Figure 19: Attachment of the stretchable membrane to the Linkam stretch stage.

3.4.1 Gauge factor and pressure sensitivity

Figure 21 A shows the relative resistance change of the device under small strain of 0-3%. The dual state behaviour possibly happens due to CNT bundles forming nano-sized gaps between each other before starting to stretch geometrically or elastically. Stretching the device much further than 3-4% would permanently increase the resistance of the device and ultimately end up breaking it completely. Impurities present in the middle of the nanotube network from CNT manufacturing process or used solvents may decrease the maximum stretching capabilities and durability of the device [15]. It is unlikely that any breakages would occur in individual nanotubes as they have very high tensile strength compared to the adhesion to other nanotubes [38].

In stretching experiments, an interesting, negative hysteresis is observed. This repeatable behaviour makes the resistance reach the stretched and unstretched states with less strain change than expected. This was also seen in earlier paper concerning piezoresistive carbon foams [39]. The reason could be cracks or gaps forming in the SWCNT network when stretching before stretching turning into geometric/elastic. On the other hand, in the releasing phase, some of the gaps close before the elastic region starts. [22] It takes time for the CNT network to reset after being stretched. Another

explanation is that the PDMS substrate contracts immediately forcing SWCNT network to contract in a different way that would be natural. [26]

The quick and linear increase of the resistance at strains of 1.0-2.5% leads to a relatively steady gauge factor of 500-1000 (Figure 21 B). A very similar result was achieved with carbon foam-based sensors [39]. In pressure sensitivity tests, the device was first pinched from the ends and set vertically in a Linkam stretch stage. Pressure over the whole device area was simulated by loading weights of 0.15 g on the top of the membrane and the resistance was measured with a DMM that uses 0.5 V voltage. The most consistent results with the least deviation were achieved by applying the pressure-simulating force as visualised in Figure 20, offset from the area where the SWCNT track is located to ensure that localized transformation of the membrane would not affect the result. As a result, the whole membrane stretched as if the pressure was applied to the whole area. This method however, does not take into account the bending of the membrane which causes the printed pattern to stretch more or less, depending on the pattern being printed on the same or the opposite side the pressure is applied to leads naturally to a higher or lower pressure sensitivity respectively.

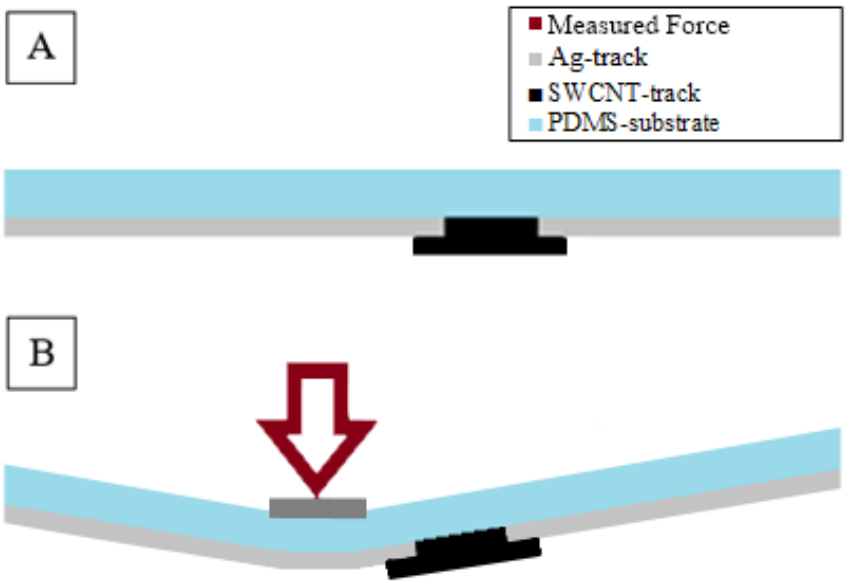

Figure 20: The pressure measurement setup with the membrane **(A)** unstressed and **(B)** stressed by an external force.

In Figures 21 C and D, The device shows very high pressure sensitivity of 100-400 kPa^{-1} being higher than that measured for the state-of-the-art CNT/rGO-CNF carbon devices. [40] The very high pressure sensitivity is explained by the membrane being very thin, floating in the air and supported only from the ends and the area affected being relatively big, about 4 cm^2.

Possible practical uses for the sensor would include pressure sensing, force measurement, buttons and human motion measurement. Apart from the silver conducting path, the device can be made almost completely transparent to the human

eye, which enables it to be used in applications where transparency is an important factor.

As the PDMS substrate is the largest counteracting force to reduce the elongation of the device, pressure sensitivity is easy to change by making the substrate different thickness from the current ~100 µm. This device would be suitable for pressure sensing applications in the range of 0-30 Pa, if the whole device was exposed to the pressure difference with only supporting it on the edges. On the other hand, by providing a better support, higher pressures are expected to be able to measure.

These results were compared with a reference sample containing no CNTs to confirm that the CNT track is the source of the effects described and that the effect of silver pattern stretching has negligible effect on the total resistance.

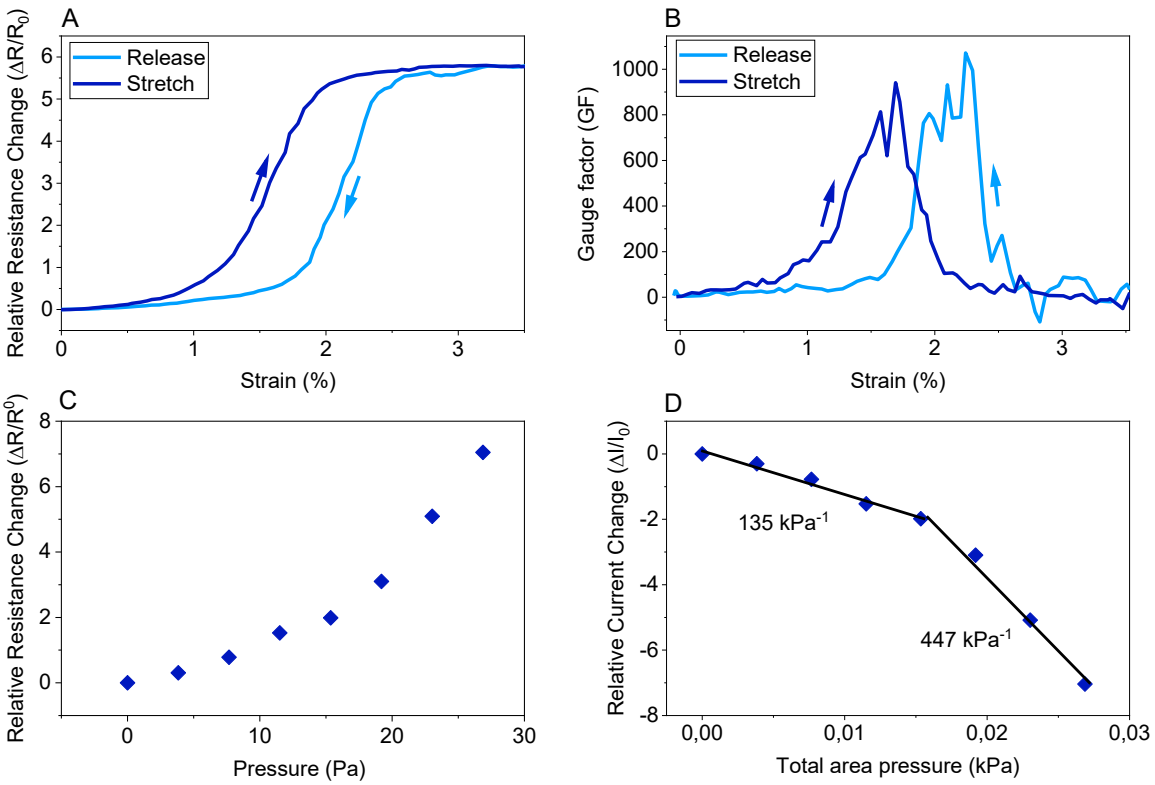

Figure 21: Fully printed SWCNT and Ag -ink based sensor on PDMS behaviour when stretched: **(A)** Resistance related to the strain, **(B)** high maximum gain factor (GF), **(C)** Resistance change related to the pressure and **(D)** Relative current change with the derivative values.

3.4.2 Sensor applications

The electrical response of the device to bending shows high sensitivity in Figure 22 A. The structure maintains its functionality even when bent under radius of 2 mm. This property could be utilized in applications that need conductors that are bendable or otherwise pliable. Other use for the resistance change would be sensors that respond

to bending, force or pressure. The CNT pattern was facing out which increases the change of the resistance. Resistance was measured with a DMM. R0 = 80 kOhm.

Figure 22 B shows the printed CNT patterns used as sensors for heartbeat (pulse) measurements without any modifications. With fine sensor placement, even different stages of the pulse could be recognized. First, the sensor was put over the radial artery and pressed manually with a finger to find the correct spot and pressure. It was then connected in series with a 22.5 kΩ wire wound resistor and a voltage of 8.74 V was sourced from Agilent E3614A voltage source. The measurement was done with an Agilent DSO-X 3024A oscilloscope. Lastly, the signal was post processed with Origin's low pass 25Hz FFT filter functionality to remove the 50 Hz mains hum from Agilent E3614A DC power supply (Figure 23).

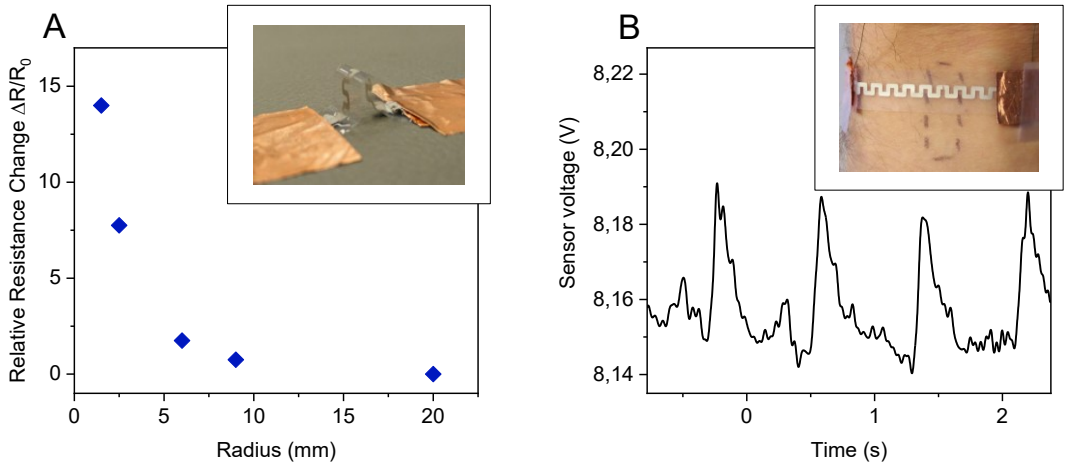

Figure 22: (A) Resistance variation of a printed SWCNT device as a function bending radius and **(B)** Radial pulse measurement with SWCNT patterns printed on PDMS to reveal various pressure fronts in pulses.

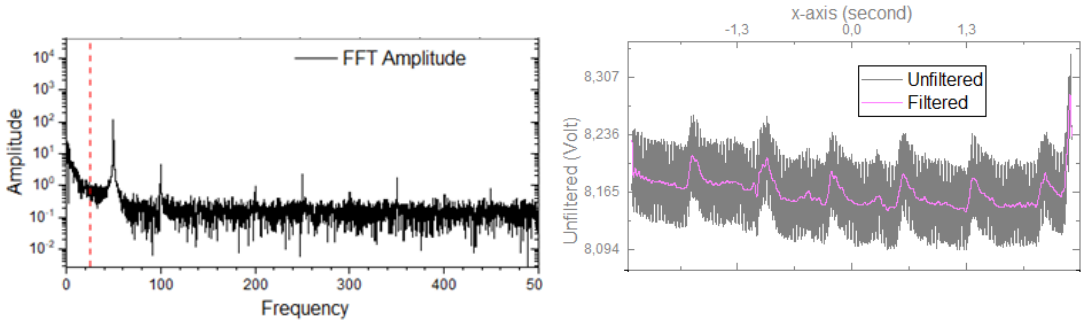

Figure 23: 50 Hz mains hum from Agilent E3614A voltage source removed with Origin 2019b low pass 25Hz FFT filter.

4 CONCLUSIONS

In this thesis, a novel SWCNT device was inkjet-printed on PDMS, measured and imaged as well as compared to other devices with similar properties.

Various SWCNT inks were prepared and used to create conductive patterns on PDMS and other substrate materials. Several phenomena affecting the printing were documented, and possible solutions for problems were discussed. The most concentrated ink containing SWCNTs in 50:50 DMF-water solution was chosen to be printed for the best conductivity in least printing time. Substrate material sourced from VTT was prepared for printing and some of them were also treated with argon plasma to optimize for subsequent inkjet-printing. With some cost in transparency and simplicity of manufacturing, the plasma treatment was found to be a successful way to increase the hydrophilicity of PDMS and thus printability on it to produce SWCNT micropatterns with controlled electrical properties. For example, decreasing number of layers needed to only one layer for a conducting pattern, or to achieve low sheet resistances of only tens of ohms when printing multiple layers.

While printing the SWCNT patterns for electrical measurements, multiple settings were varied and optimized, such as drop spacing, print repetition and surface treatment. In sensor applications, the patterns were found to have a strong piezoresistive effect with a gauge factor of up to 1000 and associated high pressure sensitivity. The printed SWCNT patterns were also demonstrated as sensors for analysing strain, bending, and pressure.

As for further development, printing of the SWCNT lines could be developed further to improve e.g. to make not only lines but also two-dimensional patterns on surfaces. It would also be beneficial to create a better protection for the SWCNT-based device to be more robust and easier to use.

There is a possibility for the device to be mass manufactured with already established screen printing and inkjet printing technologies with a relatively little investment. The SWCNT cost would be minimal due to additive style of manufacturing.

5 REFERENCES

[1] O.-H. Huttunen, T. Happonen, J. Hiitola-Keinanen, P. Korhonen and J. Ollila, "Roll-To-Roll Screen-Printed Silver Conductors on a Polydimethyl Siloxane Substrate for Stretchable Electronics," *Industrial & Engineering Chemistry Research,* vol. 58, no. 43, pp. 19909-19916, 2019.

[2] D. S. Hecht, H. Liangbing and G. Irvin, "Emerging Transparent Electrodes Based on Thin Films of Carbon Nanotubes, Graphene, and Metallic Nanostructures," *Advanced Materials,* vol. 23, no. 13, 2011.

[3] O. Pitkänen, T. Järvinen, H. Cheng, G. S. Lorite, A. Dombovari, L. Rieppo, S. Talapatra, H. M. Duong, G. Tóth, K. L. Juhász, Z. Kónya, A. Kukovecz, P. M. Ajayan, R. Vajtai and K. Kordás, "On-chip integrated vertically aligned carbon nanotube based super- and pseudocapacitors.," *Sci Rep,* vol. 7, no. 16594, 2017.

[4] S. Kumar, M. Nehra, D. Kedia, N. Dilbaghi, K. Tankeshwar and K.-H. Kim, "Carbon nanotubes: A potential material for energy conversion and storage," *Progress in Energy and Combustion Science,* vol. 64, pp. 219-253, 2018.

[5] N. Hu, Y. Karube, C. Yan, Z. Masuda and H. Fukunaga, "Tunneling effect in a polymer/carbon nanotube nanocomposite strain sensor," *Acta Materialia,* vol. 13, no. 56, pp. 2929-2936, 2008.

[6] S. Peng, K. Cho, P. Qi and H. Dai, "Ab initio study of CNT NO2 gas sensor," *Chemical Physics Letters,* vol. 387, no. 4-6, pp. 271-276, 2004.

[7] G. Toth, J. Mäklin, N. Halonen, J. Palosaari, J. Juuti, H. Jantunen, K. S. W. Kordas, R. Vajtai and P. Ajayan, "Carbon-Nanotube-Based Electrical Brush Contacts," *Adv. Mater.,* vol. 21, pp. 2054-2058, 2009.

[8] S. Sridhar, C. Tiwary, S. Vinod, J. J. Taha-Tijerina, S. Sridhar, K. Kalaga, B. Sirota, A. H. C. Hart, S. Ozden, R. K. Sinha, Harsh, R. Vajtai, W. Choi, K. Kordás and P. M. Ajayan, "Field Emission with Ultralow Turn On Voltage from Metal Decorated Carbon Nanotubes," *ACS Nano,* vol. 8, no. 8, pp. 7763-7770, 2014.

[9] E. Gracia-Espino, G. Sala, F. Pino, N. Halonen, J. Luomahaara, J. Mäklin, G. Tóth, K. Kordás, H. Jantunen, M. Terrones, P. Helistö, H. Seppä, P. M. Ajayan and R. Vajtai, "Electrical Transport and Field-Effect Transistors Using Inkjet-Printed SWCNT Films Having Different Functional Side Groups," *ACS Nano,* vol. 4, no. 6, pp. 3318-3324, 2010.

[10] K. Kordás, G. Tóth, P. Moilanen, M. Kumpumäki, J. Vähäkangas and A. Uusimäki, "Chip cooling with integrated carbon nanotube microfin architectures," *Applied Physics Letters,* vol. 90, no. 12, 2007.

[11] X. Yu, R. Rajamani, K. Stelson and T. Cui, "Carbon nanotube-based transparent thin film acoustic actuators and sensors," *Sensors and Actuators A: Physical,* vol. 132, no. 2, pp. 626-631, 2006.

[12] G. Lorite, L. Ylä-Outinen, L. Janssen, P. O., T. Joki, J. Koivisto, M. Kellomäki, R. Vajtai, S. Narkilahti and K. Kordas, "Carbon nanotube micropillars trigger guided growth of complex human neural stem cells networks.," *Nano Res.,* vol. 12, p. 2894–2899, 2019.

[13] K. Awasthi, A. Srivastava and O. N. Srivastava, “Synthesis of Carbon Nanotubes,” *Journal of Nanoscience and Nanotechnology,* vol. 5, no. 10, pp. 1616-1636, 2005.

[14] D. Warheit, “What is currently known about the health risks related to carbon nanotube exposures?,” *Carbon,* vol. 44, no. 6, pp. 1064-1069, 2006.

[15] R. H. Baughman, A. A. Zakhidov and W. A. de Heer, “Carbon Nanotubes--the Route Toward Applications,” *Science,* vol. 297, no. 5582, pp. 787-792, 2002.

[16] M. Kociak, A. Y. Kasumov, S. Guéron, B. Reulet, I. I. Khodos, Y. B. Gorbatov, V. T. Volkov, L. Vaccarini and B. H., “Superconductivity in Ropes of Single-Walled Carbon Nanotubes,” *Physical Review Letters,* vol. 86, no. 2416, 2001.

[17] B. Liu, “Performance Variation Adaptive Differential Signaling via Carbon-Nanotube Bundles,” in *Solid-State and Integrated-Circuit Technology, 2008. ICSICT 2008*, 2008.

[18] R. Jasti and C. R. Bertozzi, “Progress and Challenges for the Bottom-Up Synthesis of Carbon Nanotubes with Discrete Chirality,” *Chem Phys Lett.,* vol. 494, no. 1-3, pp. Pages 1-7, 2010.

[19] N. Komatsu and F. Wang, “A Comprehensive Review on Separation Methods and Techniques for Single-Walled Carbon Nanotubes,” *Materials,* vol. 3, pp. 3818-3844, 2010.

[20] J. Van Deun, P. Mestdagh, R. Sormunen, V. Cocquyt, K. Vermaelen, J. Vandesompele, M. Bracke, O. De Wever and A. Hendrix, “The impact of disparate isolation methods for extracellular vesicles on downstream RNA profiling,” *Journal of Extracellular Vesicles,* vol. 3, no. 1, 2014.

[21] D. L. Plata, P. M. Gschwend and C. M. Reddy, “Industrially synthesized single-walled carbon nanotubes: compositional data for users, environmental risk assessments, and source apportionment,” *Nanotechnology,* vol. 19, no. 18, 2008.

[22] L. Jin, A. Chortos, F. Lian, E. Pop, C. Linder, Z. Bao and W. Cai, “Microstructural origin of resistance–strain hysteresis in carbon nanotube thin film conductors,” *PNAS,* vol. 115, no. 9, pp. 1986-1991, 2018.

[23] S. Roth, M. Kaempgena and G. Duesberg, “Transparent carbon nanotube coatings,” *Applied Surface Science,* vol. 252, no. 2, pp. 425-429, 2005.

[24] M. Mananghaya, M. A. Promentilla, K. Aviso and R. Tan, “Theoretical investigation of the solubilization of COOH-functionalized single wall carbon nanotubes in water,” *Journal of Molecular Liquids,* vol. 215, pp. 780-786, 2016.

[25] L. Yong, W. Wanlu, L. Kejun, H. Chenguo, H. Zhi and F. Qing, “Piezoresistive effect in carbon nanotube films.,” *Chinese Science Bulletin,* vol. 48, p. 125–127, 2003.

[26] R. Zhang, H. Deng, R. Valenca, J. Jin, Q. Fu, E. Bilotti and T. Peijs, “Strain sensing behaviour of elastomeric composite films containing carbon nanotubes under cyclic loading,” *Composites Science and Technology,* vol. 74, pp. 1-5, 2013.

[27] "Dimatix Materials Printer DMP-2850," Fujifilm, [Online]. Available: https://www.fujifilmusa.com/products/industrial_inkjet_printheads/deposition-products/dmp-2800/. [Accessed 23 2 2020].

[28] T. Xu, M. L. Lam and T.-H. Chen, "Discrete Element Model for Suppression of Coffee-Ring Effect," *Scientific Reports,* vol. 7, no. 42817, 2017.

[29] "Fujifilmusa.com," Fujifilm, 16 5 2013. [Online]. Available: https://www.fujifilmusa.com/shared/bin/Dimatix_Materials_Printer_Jettable_Fluid_Formulation_Guidelines_05-13.pdf. [Accessed 11 2 2020].

[30] "Surface tension values of some common test liquids for surface energy analysis," 25 2 2017. [Online]. Available: http://www.surface-tension.de/. [Accessed 25 2 2020].

[31] J. A. Marsella, "DIMETHYLFORMAMIDE," in *Kirk-Othmer Encyclopedia of Chemical Technology*, New York, John Wiley & Sons, 2000.

[32] R. Valasma, "Micropatterned transparent conductive films of single-wall carbon nanotubes on polyethylene terephthalate surfaces," Oulu, 2019.

[33] "Does my ink need degassing?," jetXpert, 7 May 2018. [Online]. Available: https://jetxpert.com/does-my-ink-need-degassing/. [Accessed 23 2 2020].

[34] A. Eller and H. G. Flynn, "Rectified Diffusion during Nonlinear Pulsations of Cavitation Bubbles," *The Journal of the Acoustical Society of America,* vol. 37, no. 493, 2005.

[35] R. Vajtai, K. Kordas, M. Mohl, A. Dombovari and M. A. Pulickel, "Self-assembled large scale metal alloy grid patterns as flexible transparent conductive layers," *Sci. Rep.,* vol. 5, no. 1, 2015.

[36] P. Chen, H. Chen, J. Qiu and C. Zhou, "Inkjet printing of single-walled carbon nanotube/RuO2 nanowire supercapacitors on cloth fabrics and flexible substrates," *Nano Res.,* vol. 3, p. 594–603, 2010.

[37] O.-S. Kwon, H. Kim, H. Ko, J. Lee, B. Lee, C.-H. Jung, J.-H. Choi and K. Shin, "Fabrication and characterization of inkjet-printed carbon nanotube electrode patterns on paper," *Carbon,* vol. 58, pp. 116-127, 2013.

[38] M.-F. Yu, B. S. Files, S. Arepalli and R. S. Ruoff, "Tensile Loading of Ropes of Single Wall Carbon Nanotubes and their Mechanical Properties," *Physical Review Letters,* vol. 84, no. 24, 2000.

[39] K. Kordas and O. Pitkänen, "Piezoresistive Carbon Foams in Sensing Applications," *Frontiers in Materials,* vol. 6, no. 93, 2019.

[40] X. Peng, K. Wu, Y. Hu, H. Zhuo, Z. Chen, S. Jing, Q. Liu, C. Liu and L. Zhong, "A mechanically strong and sensitive CNT/rGO–CNF carbon aerogel for piezoresistive sensors," *The Royal Society of Chemistry,* no. 6, pp. 23550-23559, 2018.

[41] M. Terrones, "Synthesis, Properties, and Applications of Carbon Nanotubes," *Annual Review of Materials Research,* vol. 33, p. 419–501, 2003.